IIETA International Information and Engineering Technology Association
Advancing the World of Information and Engineering

Revue d'Intelligence Artificielle
Vol. 38, No. 6, December, 2024, pp. 1409-1422
Journal homepage: http://iieta.org/journals/ria

A Comparative Analysis of Deep Neural Networks (DNN) for Recognition of Tropical Cyclones in Real-Time Satellite Images over the Indian Sub-Continent

Manikyala Rao Tankala[1*], Venkata Bhargavi Avala[1], Monika Parnual[2], Erra Naveen Kumar[1], Srirama Venkata Gopi[1], Gera Nikita Kiran[3]

[1] India Meteorological Department (IMD), RMC-Chennai, Chennai 600006, Tamil Nadu, India
[2] India Meteorological Department (IMD), RMC-New Delhi, New Delhi 110003, India
[3] IOT Department, K.L. University, Guntur 522302, Andhra Pradesh, India

Corresponding Author Email: manik31.t@imd.gov.in

https://doi.org/10.18280/ria.380603

Received: 22 March 2024
Revised: 3 November 2024
Accepted: 3 December 2024
Available online: 21 December 2024

Keywords:
Efficient-Net neural network, training, validation, localisation, confusion matrix

ABSTRACT

Supervised learning is typically required to train a Deep Neural Network (DNN) to identify satellite cyclone images with noise and blur in the visible and infrared spectrum. This requires input-target pairs of noisy images and corresponding blurry photos. In this research, we propose a self-supervised learning method to train a Deep Neural Network (DNN) employing only real-time images from the visible and infrared spectrums. The suggested technique, which serves as a self-supervision tool, can identify convective activity, the eye of the storm, and wall clouds in the tropical cyclone cloud distribution. Our approach involves two stages: Offline pre-training on Cyclonic Storm (CS) images over the Indian sub-continent, North Indian Ocean, Arabian Sea, and Bay of Bengal was followed by real-time testing of the localization on INSAT-3D satellite images. This allows for efficient testing of the model. Satellite cyclone images of recent tropical cyclones from 2018 to 2023 are used to assess the algorithm's efficacy thoroughly. An analysis of performance metrics is attempted with graphical plots and a precision and recall matrix. Furthermore, according to the experimental results, our suggested algorithm outperforms the state-of-the-art models in terms of both classification accuracy and localization learning models' test-time performance.

1. INTRODUCTION

Recent years have witnessed a rapid advancement in the field of Remote Sensing (RS) technology. Many satellite cyclone images with varying spatial, spectral, and temporal resolutions have been acquired over the world's surface. Many thanks to the expansion of Remote Sensing platforms and the advancement of monitoring capabilities. These images constitute a substantial source of information that can be used to sway decisions in a variety of applications, such as land-cover/land-use classification, weather forecasting, urban planning, agricultural surveying, natural disaster detection, and geographic space object perception retrieval. In this manner, it is imperative from a social and economic perspective to analyse these images. Remote Sensing (RS) image classification is an important technique that divides RS scenes into groups based on the cloud distribution they contain. The RS literature contains numerous articles that address this issue, especially variants of Convolutional Neural Networks (CNN) models are used in recent state-of-the-art techniques to identify RS patterns and learn rich feature representations of them. The majority of this art work incorporates elements that completely capture the RS scene having convective cloud distribution. However, frequently only one component of that image can be used to determine which form it is part of, while the remaining constituents are either useless or belong to a diverse class. Therefore, cyclone cloud distribution elements that are necessary are considered under atmosphere storm class and remain as non-cyclonic storm class. In Figure 1, a typical RS image from the "Cyclonic Storm" class, we can see the area inside the red rectangle represents the most significant part of the picture, while the background is furnished with clutter that could potentially come from other forms.

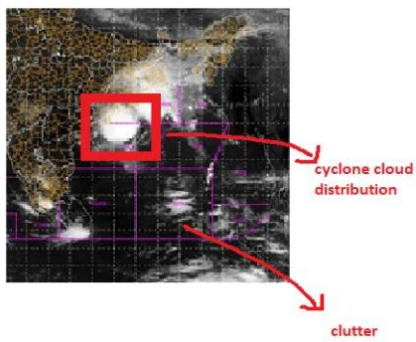

Figure 1. Satellite imagery of Jawad tropical cyclone over east coast of Andhra Pradesh and Odissa (December, 2022)

Natural language processing, object detection, image recognition, multimodal reasoning and matching, and speech recognition have all benefited from the practical application of deep learning. Moreover, these practical applications have typically made use of the attention mechanism, which remains steadfastly the fundamental concept of concentrating fiercely on particular input segments. Some proposed works that use attention are precisely applied for Remote Sensing applications such as object detection, picture segmentation, and scene classification. Figure 1 shows tropical cyclone Jawad formation over east coast of India.

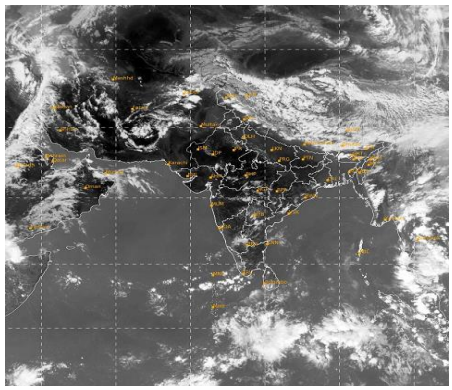

Figure 2. Satellite imagery showing non-cyclogenisis activity over India

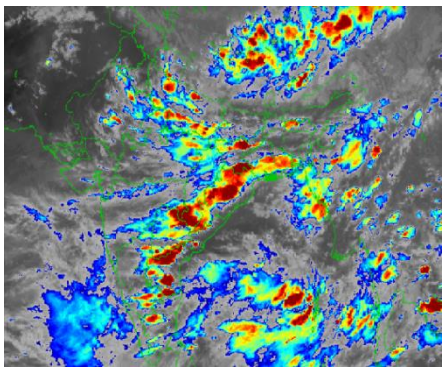

Figure 3. Convective activity over North India, coastal parts of India and over Bay of Bengal

Figures 2 and 3 show convective activity in clouds over the north and east coasts of India. Convective activity in clouds is often accompanied by heavy precipitation and thunderstorms (TS), leading to huge loss of human life and cattle, along with infrastructural damage and sometimes flash floods in waterlogged areas and hill areas. This will cause great havoc to human life, the inhabitants and animals in the forest. Hence, there is a need for automation for the recognition of convective activity in clouds, especially during cyclone formation. A cyclone is formed by wall clouds in a ring shape with convective cloud development while it changes to a severe Cyclonic Storm and even an extremely severe Cyclonic Storm. Also, this cyclone is accompanied by gusting winds and turbulence. Winds usually have speeds of more than 28 knots and may further increase during cyclone formation. In reality, a neural network is just a function approximation, and so understanding the function of activation functions in the context of deep learning requires considering this during the phase of design. Its architecture determines how well it can mimic specific function classes. The only way that input or feature vector elements interact with one another in a typical neural network is through addition. A sequence of matrix multiplications and element-wise non-linearities are used to accomplish this. The mask produced by heat map mechanisms is multiplied by features. This seemingly innocuous expansion has important consequences: Neural networks can quickly model a much wider range of functions, leading to completely new applications. In the classification of tropical cyclone images, it is important to identify the storm's eye and classify the cyclone's stage during its formation. Automating the recognition of tropical cyclones using a model could assist forecasters and meteorologists in taking necessary steps before issuing alerts to the public. This can help in estimating the location of landfall and predicting the expected precipitation in specific geographical areas. Self-supervised learning is a promising avenue for using unlabeled data and reducing dependence on costly labeled datasets; it has its challenges. The approach may falter in scenarios involving poor data quality, inappropriate pretext tasks, computational limitations, a lack of generalizability, domain-specific challenges, and issues surrounding model interpretability.

Supervised learning is still the preferred method in situations where there is a lot of high-quality labelled data, tasks have specific metrics for evaluation, interpretability is critical, computational resources are limited, domain expertise is important, and urgency and efficiency are required.

2. BACKGROUND

The following are the main characteristics of a cyclone, according to the World Meteorological Organisation: a low-pressure system with winds rotating anticlockwise (clockwise) in the northern (southern) hemisphere and a minimum sustained wind speed of 34 knots (62 kmph). For example, a Tropical Cyclone (TC), is a synoptic disturbance that spans over 100 km and is non-frontal, meaning it does not have a sharp temperature gradient. It primarily occurs over tropical or sub-tropical waters and is characterised by organised convection and distinct cyclonic surface wind circulation. The four stages of the life cycle are as follows:

(i) Formation phase (a few days)
(ii) Immature phase (1/2 day to 2-3 days)
(iii) Mature phase (1/2 day to 2-3 days)
(iv) Decaying phase (2-3 days)

Cyclogenesis is assumed to have started at the onset of depression. A cyclone's interior pressure steadily drops during its formative and immature phases as surface wind speed rises. A cyclone's top diameter increases as it forms. Throughout the mature stage, the intensity (wind and interior pressure) remains constant. However, size may increase. Moreover, during the Decaying stage, intensity decreases (wind and central pressure rise and fall). Degradation is caused by landfall, a colder sea, unfavorable atmospheric conditions, and interactions with other Tropical Cyclones (TC). Over the northern Indian Ocean, cyclones usually last five days. tropical cyclones are atmospheric disturbances brought on by the release of latent heat from the upper layers of tropical oceans. The horizontal temperature gradients in the atmosphere provide the energy source for mid-latitude cyclones.

Tropical cyclones originate from the barotropic process, which creates a small horizontal temperature gradient, whereas mid-latitude cyclones originate from the baroclinic process, which produces a large temperature gradient. The strongest winds are found closest to the surface in tropical cyclones and 8 to 12 kilometers up in the upper troposphere in mid-latitude

cyclones. Mid-latitude cyclones have cold core systems, while tropical cyclones have warm core systems. The following are important variables that affect the development of Tropical Cyclones (TC): High relative humidity levels in the lower and middle troposphere; conditional instability through a deep atmospheric layer; weak vertical shear of the horizontal winds; supply of heat and moisture through transport channels; a deep thermocline and high sea surface temperatures that exceed 26℃.

Figure 4 was utilized to apply graphical analysis and patterns to determine the T-number of cyclones. To ascertain the stages of cyclone development, this method is frequently employed during the tropical cyclone formation phase.

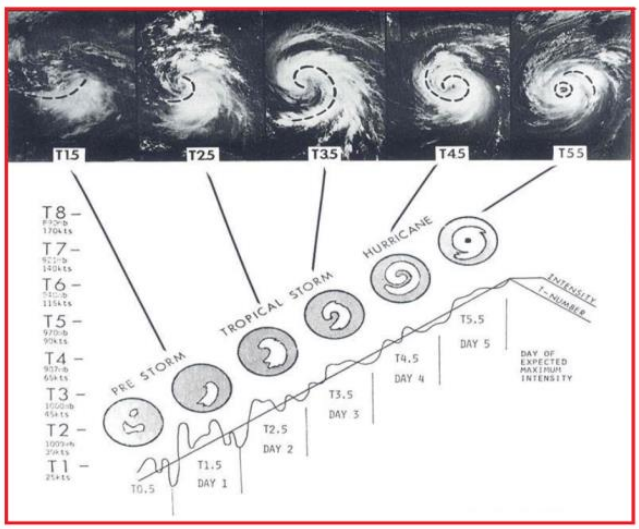

Figure 4. Tropical cyclone development analysis using T-Number and Curved patterns (Image courtesy-IMD)

Some studies of Cyclone Tracks over Bay of Bengal and Arabian Sea

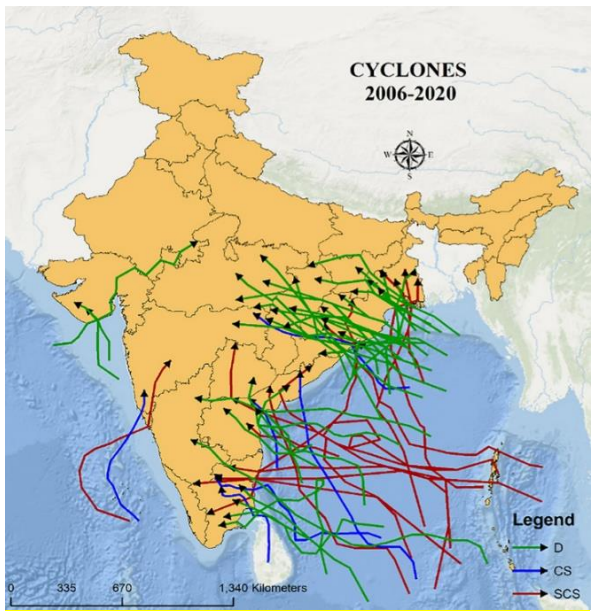

Figure 5. Climatological tracks of all cyclones developed over Bay of Bengal, North Indian Ocean and Arabian Sea

Mohapatra et al. [1-4] have discussed the formation of tropical cyclones in the Indian Ocean, tracking, and their development. Alhichri et al. [5] have discussed the classification of images using satellite imagery, but localization was not performed for eye detection in storms. Various algorithms used for classification were discussed [6-10]. Wang et al. [11] discussed the classification of low-intensity tropical cyclones very well but attained lower accuracies on distorted and blurred image data. Various algorithms mentioned in the studies [12-18] have discussed about intensification and identification of tropical cyclones and their analysis. But they have not discussed eye localisation in Cyclonic Storms. Algorithms from various fields [19-32] have discussed hyper spectral image classification in weather phenomenon. Dvorak [33] has discussed tropical cyclone intensity analysis using patterns and graphical plots. Following algorithms discuss about usage of CNN models and their variants for image classification, localization and analysis [34-44].

Further various tropical cyclone climatological tracks are shown in Figure 5 for understanding and analysis purposes. Tropical cyclones can cause a variety of potential damages, including flooding of coastal areas, injuries and fatalities, beach erosion, loss of power and communications, damage to structures, land subsidence, destruction of crops, vegetation, and livestock, flooding of inland areas, and loss of soil fertility due to saline intrusions. The reduction of cyclone disasters is contingent upon multiple factors, such as vulnerability and hazard assessments, planning and preparation, early warning systems, and mitigation. According to a survey done for the South Asian region, early warning is a crucial element. Early warning components comprise the following points

- the ability to monitor and predict cyclones,
- effectively generate and disseminate warning products,
- coordinate with emergency response units

Case study 1: Extreme Severe Cyclone Storm (ESCS)-MOCHA, May-2023

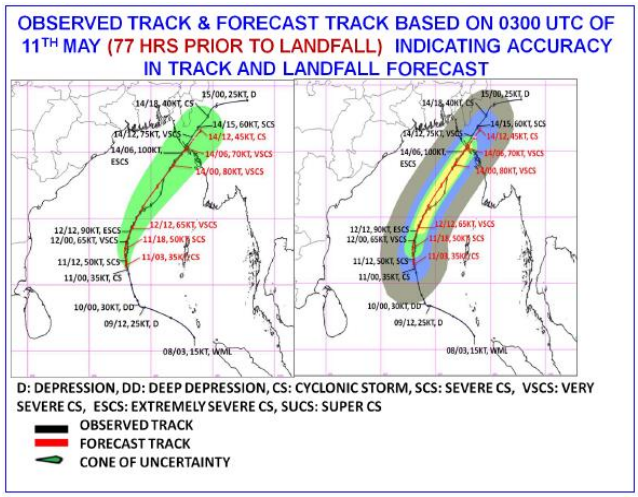

Figure 6. Typical track and intensity forecast issued on 11th May-2023 morning of Extreme Severe Cyclone Storm (ESCS) Mocha

Life History of "MOCHA":

On May 6, 2023, in the early hours of 0830 IST/0300 UTC, a cyclonic circulation developed over the Southeast Bay of Bengal (BoB) and its environs. Its influence caused a low-pressure area to form in the morning hours of May 8, 2023, 0830 IST/0300 UTC, over the southeast BoB and the nearby south Andaman Sea.

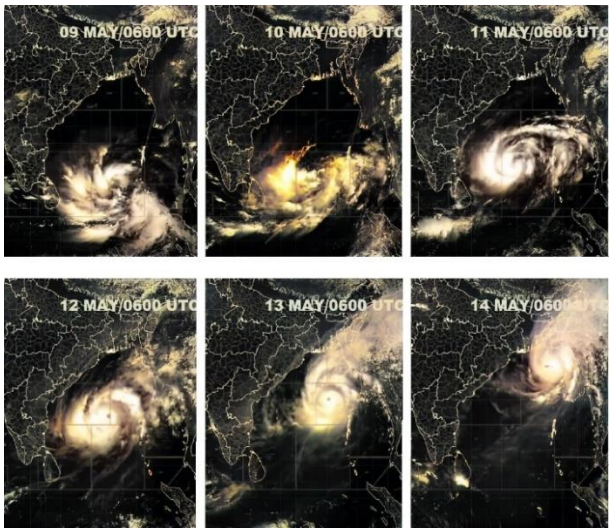

Figure 7. Satellite INSAT-3D visible imagery during ESCS Mocha (09th to 14th MAY 2023) over Indian sub-continent

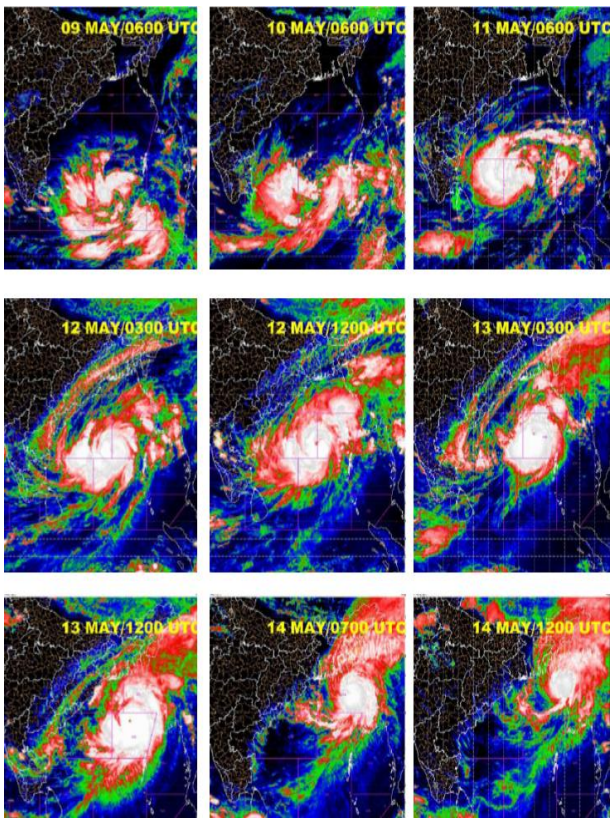

Figure 8. INSAT-3D enhanced coloured imagery during ESCS Mocha (09th to 14th MAY 2023)

It was located over the same area as a Well-Marked Low Pressure Area (WML) in the early hours of May 9, 2023, at 0530 IST/0000 UTC. That same evening, at 1730 hours IST/1200 UTC, it concentrated into a depression over Southeast BoB, with its centre located roughly 510 kilometers southwest of Port Blair. It started off moving west-northwest and strengthened into a Deep Depression (DD) over southeast BoB early on May 10, 2023, at 0530 IST/0000 UTC. Its centre was approximately 540 km west-southwest of Port Blair. After that, it headed north-northwest and strengthened into Cyclonic Storm (CS) "Mocha," also known as "Mokha," over southeast BoB early on May 11, 2023, at 0530 IST/0000 UTC. Starting at 8:30 a.m., it began to move northward on May 11 at 08:30 IST/0300 UTC and strengthened into a Severe Cyclonic Storm (SCS) over the same area in the evening of May 11 at 17:30 IST/ 1200 UTC. Later on, in the early hours of May 12 (0000 UTC/530 IST), it began to gradually recurve north-northeastward and strengthened into a Very Severe Cyclonic Storm (VSCS) over central BoB. As it continued to move north-northeast, it strengthened into an Extremely Severe Cyclonic Storm (ESCS) over east-central BoB at midnight on May 12 (2330 hrs IST/ 1800 UTC). It continued to intensify until the early hours of May 14th, moving north-northeast. Peak intensity occurred over the east-central BoB between midnight on the 13th and early morning on the 14th, with gusts reaching 240 kmph.

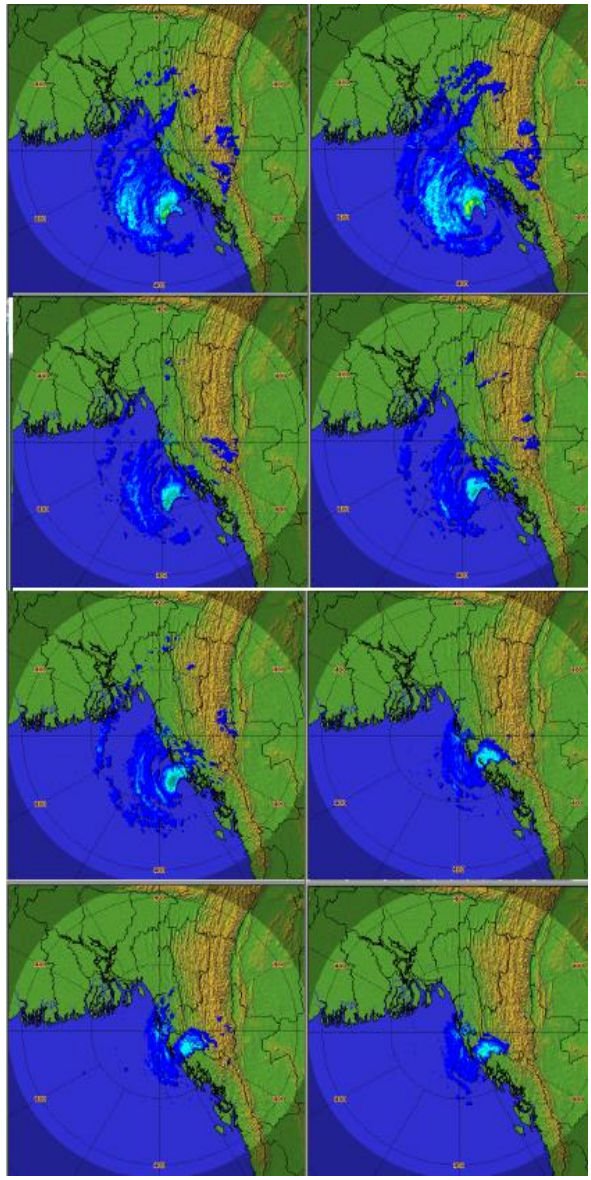

Figure 9. Cox's Bazar radar images, Bangladesh during landfall of ESCS Mocha dated 14 May, 2023

Next, it weakened slightly and moved across the coasts of north-eastern Bangladesh and north-western Myanmar between Kyaukpyu, Myanmar, and Cox's Bazar, Bangladesh, near Sittwe, Myanmar. It was an ESCS with a maximum sustained wind speed (MSW) of 180–190 kmph, gusting to 210 kmph between 1230 and 1430 hours IST on May 14, (0700 UTC to 0900 UTC). After that, it weakened into a VSCS over west-central Myanmar in the evening (1730 hrs IST/ 1200 UTC), a SCS over the same area in the night of May 14 (2030

hrs IST/ 1500 UTC), and a CS over west-central & adjoining northwest Myanmar in the early hours of May 15 (0230 hrs IST of May 15/ 2100 UTC). It continued to move north-northeastwards after that. After that, on May 15, early in the morning (0530 hrs IST/0000 UTC), it moved west-northwestward and quickly weakened into a depression over northwest Myanmar. The observed track of the system is presented in Figure 6, Figure 7 and Figure 8 shows satellite imagery of MOCHA cyclone.

Radar imagery of ESCS MOCHA is shown above in Figure 9 during the landfall phase on May 14, 2023. Further, these images were used for nowcasting during the landfall. These images were also helpful in finding convective activity in cloud distribution and for precipitation assessment in a particular location of choice. Figures 10 & 11 (a-b) show damage caused after landfall of cyclone.

Figure 10. (a) Extensive damage to huts in Rakhine state of Myanmar, (b) Collapsed roof tops, Rakhine (c) damaged houses at Basra camp, Sittwe, Myanmar (Radio Free Asia, and (d) damaged buildings & trees in Rakhine, Myanmar

Figure 11. (a) Damaged home at Saint Martin Island in Cox's Bazar, Bangladesh (b) Rescue workers clearing roads in Teknaf

According to reports from the Myanmar media (Associated Press Television News, May 19), 145 people died in Myanmar as a result of the ESCS MOCHA. In Myanmar, it resulted in extensive damage to buildings, cell phone towers, trees, and other infrastructure, as well as widespread flash floods and power outages. A few images showing damage are located in Figure 10. The effects of "MOCHA" were also felt in southeast Bangladesh's neighbouring regions. The combination of high winds and persistent rain caused damage to numerous houses and the fall of trees. Nevertheless, Bangladesh did not report any deaths. Figure 11 displays a few related damage photos from Bangladesh. In India, no damage has been reported from Andaman & Nicobar Islands. However, Mizoram state received the burnt from “ESCS MOCHA”.

Case study 2: Extreme Severe Cyclone Storm (ESCS)-Michuang, December, 2023

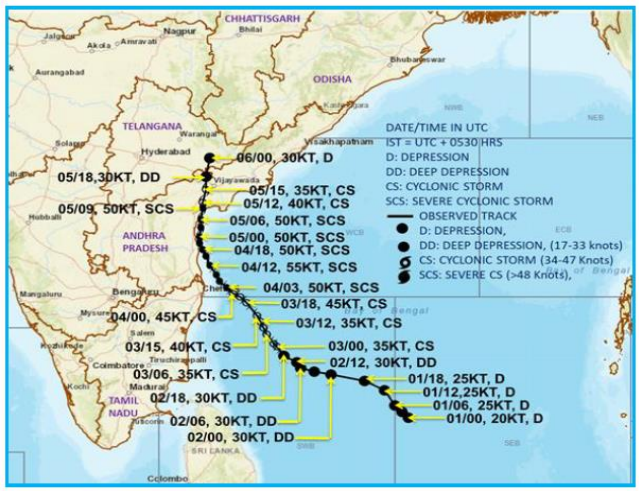

Figure 12. Severe Cyclonic Storm "Michaung" was tracked over the Bay of Bengal, December, 2023

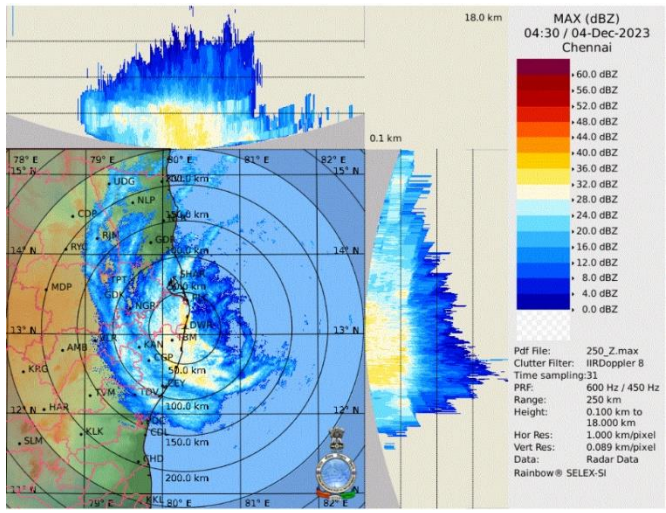

Figure 13. Doppler weather radar imagery of DWR-Chennai, showing activity of Severe Cyclonic Storm (SCS) MICHAUNG on 04th December, 2023

Life History of “MICHAUNG”

Early on November 26, at 0830 IST /0300 UTC, a cyclonic circulation formed over the South Andaman Sea and the South Thai border. Early on November 27, at 0530 hours IST/0000 UTC, a low-pressure area developed over the South Andaman Sea and the nearby Malacca Strait due to its influence. It was located in the early hours of November 29 (0530 IST/0000 UTC) over the Southeast Bay of Bengal and the South Andaman Sea as a well-marked low-pressure area. It moved westward and, early on December 1, 2023, at 0530 hours

IST/0000 UTC, concentrated into a depression over Southeast and the Southwest Bay of Bengal. Early in the morning, it moved west-northwestward and strengthened into a Deep Depression over Southwest Bay of Bengal. It developed into a Deep Depression over Southwest Bay of Bengal in the early hours of December 2, 2023, at 0530 hours IST/0000 UTC, after moving west-northwestward. Proceeding in the same direction, on December 3, 2023, early in the morning (0530 hours IST/0000 UTC), it strengthened into a Cyclonic Storm "MICHAUNG" (pronounced as MIGJAUM) over the southwest Bay of Bengal. Figures 12 & 13 show the track of cyclone and radar images tracked during formation and landfall of cylone.

Then, in the forenoon of December 4th (0830 hours IST/0300 UTC), it moved northwestward and intensified into a Severe Cyclonic Storm over the Westcentral & adjoining Southwest Bay of Bengal off the coasts of south Andhra Pradesh and adjacent north Tamil Nadu.

After that, on December 5, 2023, between 12:30 and 14:30 IST (0700-0900 UTC), it moved almost exactly northward, almost parallel to the coast of south Andhra Pradesh, and crossed it between Nellore and Machilipatnam, near Bapatla. At that time, it was classified as a Severe Cyclonic Storm, with a maximum sustained wind speed of 90–100 kmph gusting to 110 kmph. Following landfall, it proceeded to move almost straight north before weakening into a Cyclonic Storm. It was centred over south coastal Andhra Pradesh, roughly 15 km west of Bapatla, at 15:30 IST/1000 UTC on December 5. After that, it headed north-northeast and weakened, first into a Depression and then into a Deep Depression over coastal Andhra Pradesh at around midnight on December 5 (2330 IST/ 1800 UTC). Further into a Depression in the early hours of December 6th (0530 IST/0000 UTC) over northeast Telangana and surrounding regions of south Chhattisgarh, south Odisha, and coastal Andhra Pradesh. In the forenoon of December 6th (0830 IST/ 0300 UTC), it weakened into a clearly defined low pressure area over the same region. In the morning of December 7, it weakened into an upper air cyclonic circulation over Odisha, and on December 8, it became less noticeable.

Figure 14. Submerged cars in flooded Chennai during MICHAUNG cyclone Tamil Nadu, India

Media reports state that 17 people died in various "Michaung"-related incidents in Tamil Nadu and two in Andhra Pradesh. Over 41,000 individuals were evacuated and temporarily relocated, comprising 32,158 in Tamil Nadu and 9,500 in Andhra Pradesh. Chennai experienced flooding and heavy rain, forcing the closure of schools and offices, as shown in Figure 14. Field flooding in Andhra Pradesh and Odisha has resulted in reports of crop damage and losses, which are shown in Figure 15. The images of the damage from Andhra Prades, Tamil Nadu, Odisha were displayed.

Figure 15. Damaged crops in Malkangiri district of Odisha, India

Water becomes a hazard when there is too much, or too little, or if the quality is poor. During a cyclone, there is too much water, damaging almost everything that encounters it. And after the event, it leaves the water resources contaminated, making them unusable. Considering the above two case studies and the goal of reducing the fatalities of humans and animals, there is a need for automation in the prediction of satellite images with the growth of Tropical Cyclone [TC] cloud distribution in the atmosphere over the Indian Subcontinent.

Zheng et al. [18] have employed the attention mechanism for cloud detection, adopting the Cloud-AttU model on the Landsat-8 dataset provided by the National Aeronautics and Space Administration (NASA). The Cloud-AttU model accomplished an overall accuracy of 97.05%. The model has achieved good performance in detecting clouds based on snow and ice in the upper atmosphere and failed to recognize convective clouds. Other algorithmic models include Cloud-net, U-Net, FCN (Full Convolution Network), FMask (Function of Mask), and CNN (Convolution Neural Network), which all have achieved general accuracies of less than 96.13%. Rajesh et al. [32] adopted the DLR-FH model (dichotomous logistic regression fuzzy hypergraph) for satellite cyclone cloud classification, and an accuracy of 98% was achieved. The localization of cloud distribution was not performed while implementing this algorithm. Shakya, Kumar, and Goswami [20] have utilized Sequential CNN, NasNet Mobile, and MobileNet for satellite cloud recognition and classification but have achieved an accuracy of 97% only and haven't performed localization on clouds. Similarly, Jiayi Li et al. [22] used the VGG-16 model and achieved 77% precision. Pang et al. [17] used DCGAN and YOLO-v3 models for satellite cloud recognition and achieved a validation accuracy of 98%.

In this study, we present a deep learning approach for categorizing the distribution of satellite clouds in the visible and infrared spectrum. Our method integrates the newly developed Efficient-Net model with a heat map mechanism. Specifically, we introduce the EfficientNet-B3-Attention CNN, a modified version of the EfficientNet-B3 CNN that incorporates an additional branch for learning a set of weights for combining convolutional features in the intermediate layers

of the network. The selection of the optimal intermediate layer is based on the results of our experiments.

The following are some of the paper's significant contributions:

1) Based on the Gradient class activation heat mapping and the EfficientNet-B3 CNN model, we suggest a method to categorise satellite Cyclonic Storms during classification.

2) To assess the efficacy of the proposed EfficientNet-B3 model, we test it using data from recent cyclones that occurred in the North Indian Ocean, Bay of Bengal Arabian Sea.

3) Localisation of Cyclonic Storm images is done using the model so obtained.

4) Prediction of satellite images for the presence of Spiral Cyclonic Cloud distribution with convective activity and gale winds.

The remaining sections of the paper are arranged as follows: The family of Efficient-Net CNN models is described in Section 2, along with the suggested technique in Sections 2.6 and 2.7. We then give the datasets used and the outcomes of the experiments in Section 3. Section 4 presents the findings and potential directions for further investigation.

2.1 Steps of proposed method using Deep Neural Networks

The basic steps of algorithm have been shown in below Figure 16 which gives information about workflow.

Step 1: Feature extraction of images.

Step 2: Training & Testing of real-time satellite images.

Step 3: Evaluating the performance metrics on the dataset of tropical cyclones.

Step 4: Plotting the curves and Tabulation of performance criteria.

Step 5: Prediction of tropical cyclone cloud distribution in the images of infrared and visible spectrum.

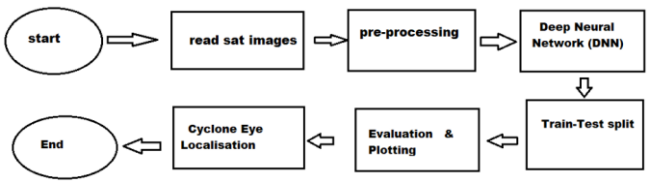

Figure 16. Block diagram of proposed algorithm

2.2 Basic structure of CNN (Convolutional Neural Networks)

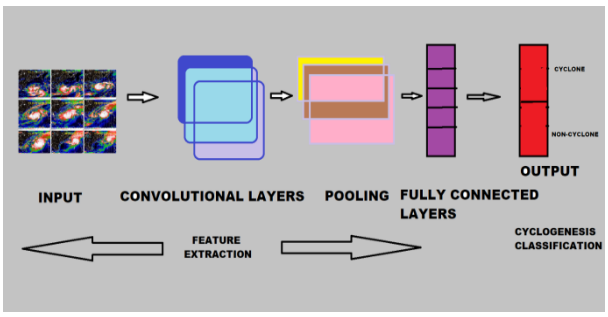

Figure 17. Convolutional Neural Network (CNN) structure

Convolutional Neural Networks (CNN) is a type of deep learning model for processing grid-patterned data and images, and has been shown in Figure 17. From low-level patterns to high-level ones, the goal is for it to automatically and adaptively learn the spatial hierarchies of features. Convolution, pooling, and fully connected layers are the three main types of layers (or building blocks) that make up a CNN in mathematics. The final layer handles classification, while the first two—the convolution and pooling layers—perform feature extraction. A convolution layer is crucial to CNN. Convolution is one type of linear operation among many mathematical operations that make up CNN.

2.3 Using Residual Neural Network (ResNet -50)

Convolution, batch normalization, and pooling operations make up the majority of the ResNet architecture shown in Figure 18. These operational blocks are repeated for each input image that is processed for a classification task. The layer's width and height don't change during this process. Usually, 64, 128, 256, and 512-pixel images were subjected to 3*3 convolutions. The ResNet model merely employs skip connections in the signal processing phase, and stride movement is utilized to achieve layer reduction. The 50 layers of the ResNet 50 model use average pooling, normalization, and 48 convolutional blocks. The ResNet-50 architecture was obtained by replacing a 3-layer bottleneck block for each of the 2-layer blocks in ResNet 34. The residual blocks with skip connections that make up the majority of the model play a vital role in classification. Using 'Imagenet' weights, categorical cross-entropy as the loss function, "softmax" as the activation function, and a learning rate of 0.01 is the optimization process carried out by the Adam optimizer.

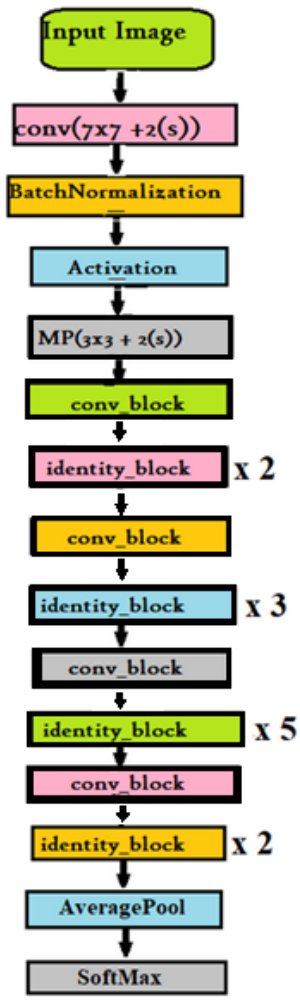

Figure 18. Block diagram of Residual Neural Network (ResNet-50) with 50 layers

2.4 Using Vision Transformer (Vi-T) neural network

Linear embedding, transformer encoder, and multi-layer perceptron are parts of Vision Transformers (Vi-T) [21]. The input images from satellite are split up into equal parts of small, identically sized patches. These patches are then flattened and transformed for lower-dimensional linear embedding values. During the classification task, the transformer encoder receives these embedding values for comparison. Ultimately, the Transformer is optimised for the classification of images. After training the model for 50 epochs, a training loss of 2.2262 exponential -09 is achieved, and a training accuracy of 100% is obtained. The period of computation is 117 minutes, and during the testing phase, a validation loss of 0.464 is obtained with a validation accuracy of 98%. Categorical cross-entropy as a loss function, Adam optimizer, and RELU (rectilinear unit) as activation functions were used during training and testing with a batch size of 2048. The encoder is shown in Figure 19.

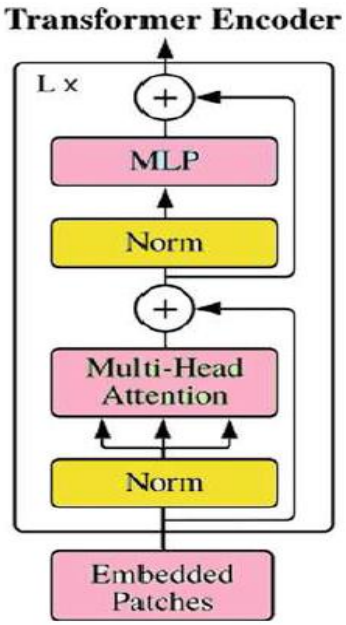

Figure 19. Encoder used in Vision Transformer (Vi-T) neural network

2.5 Using hybrid features and random forest classifier

In this section, we look at the HSV and LUV colour spaces and talk about how to extract a colour feature vector. To create a hybrid colour feature vector that is used to train and test a classifier, these colour features are extracted from each image and concatenated. The three channels in the HSV colour model are hue, saturation, and value, or intensity. The "colour" can be represented by the Hue channel. For example, the colour "red" is a colour. Red, both light and dark, is not a colour. The saturation channel is used to measure the degree of colour distinction. The brightness and intensity of a colour (light green or dark green) match.

The luminance component is represented as "L" in the LUV colour space, which is an analogue representation of colour space. The U,V Chroma components are created by subtracting the channels from the original image. The final step is to combine the two colour spaces to create a hybrid feature, which is then converted to a numerical value to create a feature vector. The classifier is trained using this feature vector. Satellite cyclonic cloud distribution images are given class labels of 1, and images with no cyclonic cloud distribution are given class labels of 0. Additionally, a pixel matrix is created by taking into account all 1000 images in the dataset. Each image is combined with a class label to create a raw image vector. It is a tree-based ensemble learning algorithm. To build the decision trees that comprise the Random Forest Classifier, a randomly selected subset of the training data was used. To determine the final class of the test object, it aggregates the votes from multiple decision trees. The number of classification trees used depends on the number of estimators used in the classifier. The benchmark dataset is split into training and testing samples and validated using 10-fold cross-validation in order to obtain the assessment metrics. Below is a list of a few benefits of the Random Forest classifier.

a. It is among the most accurate learning algorithms available. It results in greater accuracy for different datasets.

b. Performs admirably on large datasets.

c. It has a greater capacity for variable evaluation.

d. When categorising, it enables the estimation of important variables.

2.6 Using EfficientNet-B3 models

In addition to examining the connection between CNN models' breadth and depth, Tan and Le [19] have produced a workable technique for developing CNN models with fewer parameters and improved classification accuracy. In their initial research, they proposed seven of these models under the heading of "Efficient Net CNN models," which they called EfficientNet-B0 through EfficientNet-B7. Tan and Le [19] show that the Efficient Net CNN models outperform all previous models in terms of parameter count and Top-1 accuracy when applied to the ImageNet dataset. The architecture of the EfficinetNet-B3 model, which consists of multiple layers for processing input images for classification, is depicted in Figure 20.

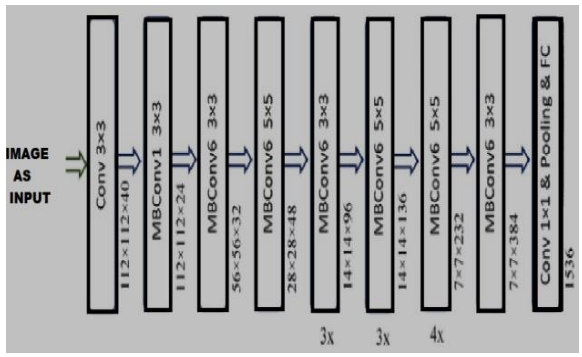

Figure 20. Architecture of EfficientNet neural network – B3 model for satellite tropical cyclone image classification

Squeeze optimisation, excitation protocols, and Mobile Inverted Bottleneck Convolution (MBConv) make up the EfficientNet architecture. MBConv uses the 1×1 convolution method to expand the channel before applying a deep convolution operation to each image. Deep convolution is converted into a feature map by applying a convolution method with d×d cores to each image channel. Every layer passes through the Swish function of the enable function. Unlike the Swish, Tanh, and Sigmoid functions, it prevents the gradient value from saturating near zero during the learning process. The extracted feature map is replicated using a feature map that excludes the compression and excitation layer in

order to highlight significant features. Lastly, the channel's scale is decreased using a 1×1 convolution process.

2.7 Using EfficientNetV2-s neural network

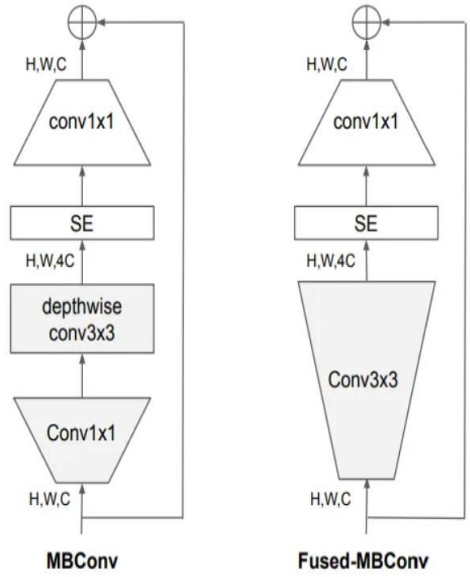

Figure 21. Structure of EfficientNetv2s model

The EfficientNetV2s models were examined within the expanded search space that included new operations like Fused-MBConv. While being six times smaller, EfficientNetV2s shown in Figure 21, models train data significantly faster than state-of-the-art models. Scaling and training-aware neural architecture search (NAS) work together to maximise both parameter efficiency and training speed.

The original MBConv in EfficientNet-B4 is gradually replaced by Fused-MBConv. Fused-MBConv can increase training speed in stages 1-3 while incurring a minimal overhead in terms of parameters and FLOPs. Both MBConv and the recently introduced fused-MBConv are heavily utilised in the early layers of EfficientNetV2. For MBConv, EfficientNetV2 favours smaller expansion ratios because they typically result in lower memory access overhead. Thirdly, although EfficientNetV2 favours smaller 3×3 kernel sizes, it increases the number of layers to offset the smaller kernel size's decreased receptive field. Finally, the final stride-1 stage in the original EfficientNet is eliminated entirely in EfficientNetV2, possibly as a result of its high parameter size and memory access overhead.

3. DATASET

The different cyclones, formation times, and number of images taken into consideration for dataset formation during experimentation are shown in Table 1.

Table 1. Dataset comprising names of various cyclones and period of formation

S.No.	Names of Cyclones	Period	Total Number of Images
1	Michuang (SCS), Biparjoy (ESCS), Tej (ESCS), Mocha (ESCS), Tej (SCS), Mandous, Asani (SCS), Yaas (VSCS), Tauktae (ESCS) Gulab (CS), Jawad (CS), Sitrangi (CS) Nivaar (CS), Shaheen (SCS)	2018-2023 (last 6 years)	3950 images of INSAT-3D Visible and IR spectrum images

SCS – Severe Cyclonic Storm, CS-Cyclonic Storm, ESCS-Extreme Severe Cyclonic Storm VSCS-Very Severe Cyclonic Storm, CS-Cyclonic Storm, BoB-Bay of Bengal, AS-Arabian Sea, DD-Deep Depression;

3.1 Evaluation metrics

Through 10-fold cross-validation against a dataset of satellite images, the performance of neural network classification is assessed using a confusion matrix (2*2 matrix). The provided dataset is divided into ten parts for 10-fold cross-validation; nine of these parts are used to improve the model and one is implemented for testing. Accuracy, sensitivity, precision, sensitivity/recall, and F1-score are computed from the true-positive (TP), false positive (FP), true-negative (TN), and false negative (FN) values in the confusion matrix. The formulas listed at the end are employed to calculate these parameters. Eqs. (1)-(4) show the metrics for binary classification of INSAT 3D and 3DR satellite imagery, respectively. Table 2 compares evaluation metrics with various classifiers.

Table 2. Hyper-parameter values using Vi-T neural network

Learning Rate	Number of Epochs	Training Accuracy	Validation Accuracy	Loss	Period of Computation
0.01	50	100%	98 %	0.464	117 minutes

$$Accuracy = \frac{TP+TN}{TP+TN+FP+FN} \quad (1)$$

$$Precision = \frac{TP}{TP+FP} \quad (2)$$

$$Recall/Sensitivity = \frac{TP}{TP+FN} \quad (3)$$

$$F1\text{-}Score = \frac{2*Precision*Recall}{Precision+Recall} \quad (4)$$

3.2 Advantages of the model

The model was used to predict the presence of tropical cyclone clouds and cyclone image classification which was evaluated with a testing accuracy of 98%. In the prediction phase, the created model withstood the presence of noise, rotation and shift in cyclone images. The proposed method generated more accurate results in less time and an image dataset was used to plot the precision and recall matrix.

Further, higher sensitivity and precision were achieved during training and testing on satellite image datasets with validation of 20%. Also F1-score (Harmonic mean of Eq. (2) and Eq. (3) of 0.97 is achieved on real-time satellite imagery of INSAT-3D. Model robustness and efficiency are verified thoroughly on new images and outcasts the state-of-the-art methods in deep learning.

3.3 Software and Hardware used

The algorithm was computed using an i5 processor with 8 GB of RAM and an NVIDIA 1050 graphics card. Python programming is used to create algorithms, and the Numpy, Scipy, and Matplotlib libraries were used for mathematical analysis. The Jupyter Notebook IDE implemented the algorithm using deep learning frameworks like Tensorflow & Keras as the platform.

4. RESULTS AND DISCUSSION

4.1 Using ResNet-50 and U-Net

The ResNet-50 model achieves a 96% Validation accuracy rate with "Adam" acting as the optimizer, "ReLu" as the activation function, and a learning rate of 0.01 on the satellite imagery dataset. Moreover "Imagenet" weights were chosen during the cyclonic image training and validation processes. Categorical cross-entropy is used as a loss function. An additional split of the train test is made as 80% & 20% for evaluation. The soft-max layer performed classification on the satellite imagery during the categorization of tropical cyclones. Adam Optimizer performed well while calculating the gradient and it avoided the vanishing gradient problem and the presence of noise in satellite imagery. The primary advantage of this algorithm is that it took less number of epochs i.e.,6 with input image dimension as 224*224. F1-Score (geometric mean of precision & recall) 0.95 was obtained and has well localized the Eye of Tropical Cyclones using the Grad-CAM technique further, the inference time obtained is less than 20 milliseconds. Both ResNet model and U-Net performed well with respect to training accuracies but have shown lower F1-score after validation on satellite imagery.

4.2 Vision transformer (Vi-T) neural network

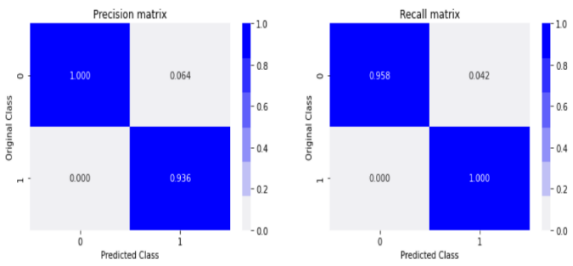

Figure 22. Precision and Recall matrix obtained on satellite imagery using Vi-T network (Vision Transformer neural net)

Vision Transformer attained good validation accuracy when compared with other networks but at the cost of training which conducted more time for training i.e., for 50 epochs. Significantly, it has to be fine-tuned for more number of parameters (85 million) when compared to ResNet-50. Around 97% of validation accuracy is obtained with a batch size of 2048, learning rate of 0.001, MLP (Multi-Layer Perceptron) size of 3072, and hidden size of 768. Further lesser inference time is obtained for the Vi-T neural network. The F1-Score obtained is appreciably good of value 0.98. Table 2 shows evaluation metrics of classification using Transformer. Precision and Recall matrix obtained on satellite imagery using Vi-T network shown in Figure 22.

4.3 Using random forest algorithm and hybrid features

Image classification with the random forest algorithm attained good accuracy during the evaluation phase with 5-fold cross-validation; further, the inference time was lower compared with other algorithms during the testing phase, which is an advantage, but it took more time for the training phase. Figure 23 shows the confusion matrix which is obtained after random forest classifier usage on the image dataset.

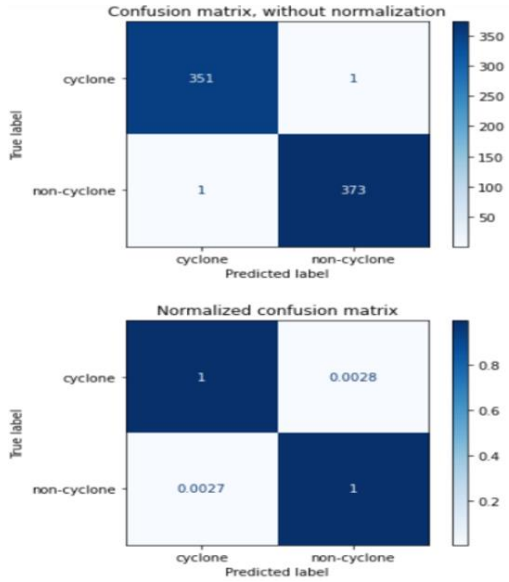

Figure 23. Confusion matrix obtained during evaluation with hybrid features & random forest classifier

4.4 Using Efficient-Net B3 & Efficient-Net-v2S models

The precision and recall matrixes for the Efficient-B3 and Efficient-V2S models at the classification evaluation stage are displayed in Figures 24 and 25. Regarding the accuracy of validation against the existence of distortion and blur in satellite imagery, they both fared well. Moreover, Efficient-V2S required less time in the prediction stage than the other models that were employed in the investigation. Efficient-Net models make extensive use of depth wise separable convolutions, which help to reduce model size and computational cost while maintaining the ability to learn rich feature representations. This enables the network to extract and generalise critical features from two different classes of satellite images, including complex image scenes of cloud distribution. Transfer learning and fine-tuning improve Efficient-Net's generalisation ability even more. Pre-trained on a large dataset such as ImageNet, Efficient-Net models have learned a diverse set of features applicable to a wide range of image classes. When fine-tuned on a specific dataset with two classes, these models adapt quickly and improve their ability to distinguish between those classes only. Further, re-training is not required while performing generalization process.

Table 3. Compares all deep neural networks using performance metrics obtained during the evaluation phase

S.No.	Algorithm	Training Accuracy	Testing-Accuracy	F1-Score	Inference Time	Avg Time -Computational Efficiency per Each Step
1	ResNet-50	99%	96%	0.82	900 milli sec	85s
2	U-Net	98%	94%	0.81	950 milli sec	90s
3	Efficient-Net-B3	98%	94%	0.94	390 milli sec	125s
4	Efficient-NetV2s	99%	97%	0.95	750 milli sec	95s
5	Dense-Net	97%	95%	0.90	700 milli sec	90s
6	Vision Transformer (Vi-T)	99%	97%	0.94	500 milli sec	100s
7	Hybrid features + Random forest	98%	97%	0.96	600 milli sec	80s

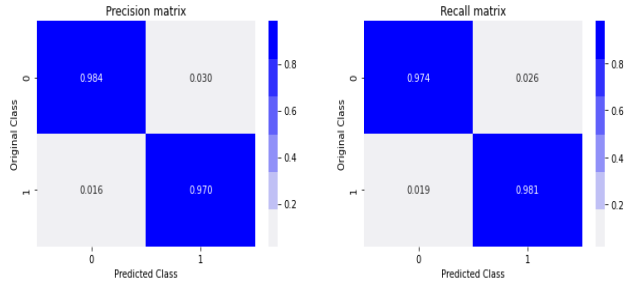

Figure 24. Precision and Recall matrix obtained after tropical cyclone classification using the efficient Net B3 model

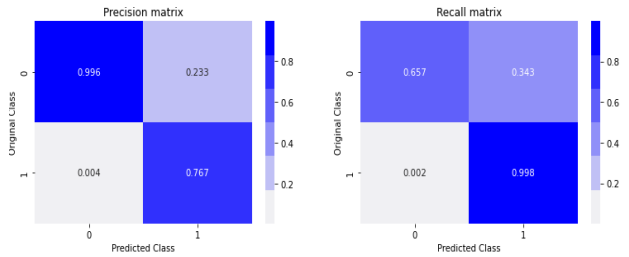

Figure 25. Precision and Recall matrix obtained on EfficientNetV2s neural network after classification

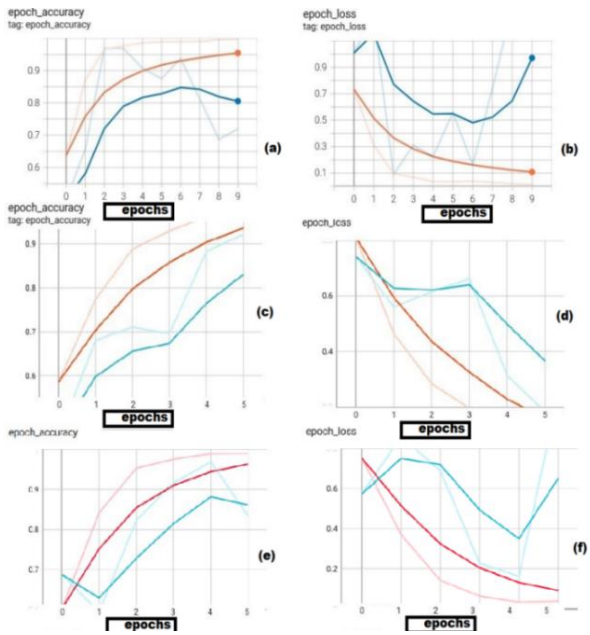

Figure 26. Training vs validations accuracies plots & loss plots

(----------**Training curve** and ----------**Validation curve)**

Figure 26 shows plots of models obtained during training and validation phases on a satellite imagery dataset using Tensorboard, and Table 3 depicts a comparison of various algorithms used in this paper with respect to F1-Scores and accuracies and inference times.

The models' predictions during the validation phase and their resilience to different attacks, such as blurring and adding noise to input images during the evaluation phase, are displayed in Figures 27 and 28. As a result, in the validation stages, the models that were acquired after training have demonstrated improved performance against image distortion. The models have an average accuracy of 98% in predicting the convective growth of tropical cyclones.

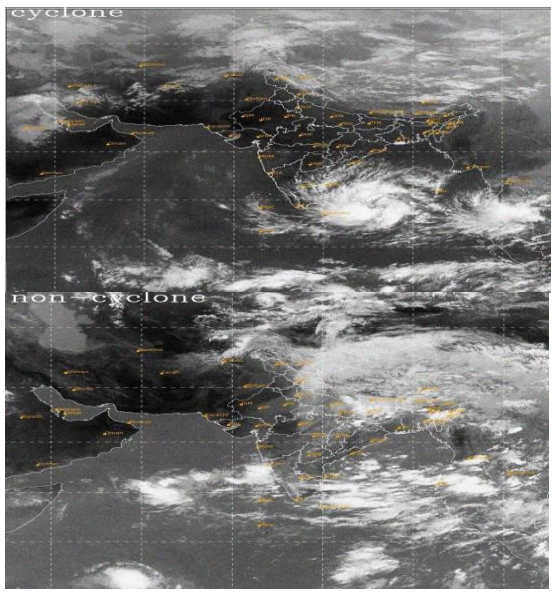

Figure 27. Model prediction outputs after training on dataset indicating labels of cyclone and non-cyclone

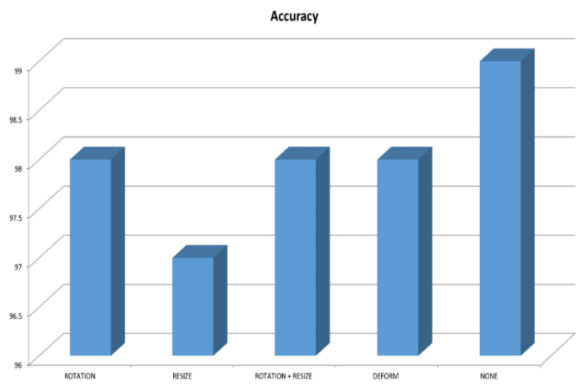

Figure 28. Comparison of accuracies on image deformations

Figure 29 shows a comparison of accuracies after training

and testing using various algorithms. Table 4 lists several algorithms for classifying satellite imagery. It is quite obvious that the suggested algorithm outperforms the other cutting-edge techniques in terms of classification accuracy and Tropical Storm Eye localization. As a result, the suggested Efficient-Net algorithms are highly suitable for identifying the emergence of convective clouds in tropical cyclones and regions of precipitation, which is very beneficial for forecasting. Additionally, the suggested approach is tested and trained on graphics hardware.

Table 4. Comparative analysis with state of art methods for Tropical Cyclone (TC) Image classification

S.No.	Method	Author	Metrics	Dataset	Cyclone Eye Localisation
1	Adhoc CNN	Sharma et al. [16]	Accuracy: 99%	ERA interim,CAM5.1,NCEP-NCAR	No
2	U-Net	Kumler-Bonfanti et al. [29]	Accuracy: 99%	GFS(mod)	No
3	Adhoc CNN	Shakya et al. [20]	Accuracy: 97%	KALPANA-I (sat) & MOSDAC (sat)	No
4	RetinaNet & Polynomial Regression	Shakya et al. [20]	RMSE: 5%-15.55%	KALPANA-I (sat) & MOSDAC (sat)	No
5	DeepLabv3+	Prabhat et al. [43]	IOU: 0.2441	CAM5.1(mod 25km)	No
6	DCGAN and YOLO v3	Pang et al. [17]	97.78% and Map@IoU=0.5: 81.39%	Satellite Images from NII (Visible)	No
7	Dichotomous Logistic Regression Based Fuzzy Hypergraph model	Rajesh et al. [32]	98.59 %	Satellite images 10 to 100	No
8	Efficient Net	Our Study	Accuracy 98%	INSAT 3D Satellite imagery using Visible and IR Spectrum	Yes

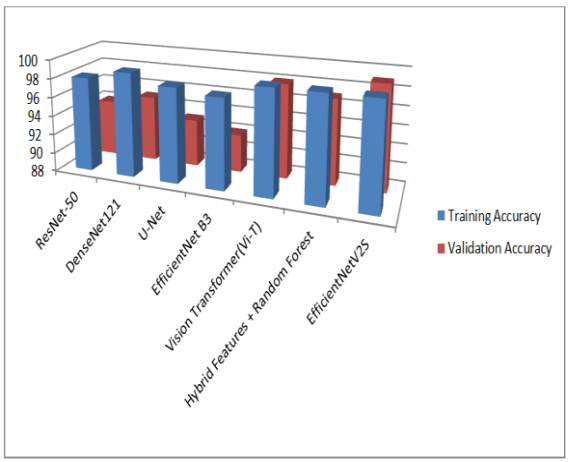

Figure 29. Comparative analysis of deep learning algorithms using accuracies

4.5 Localisation using gradient mapping

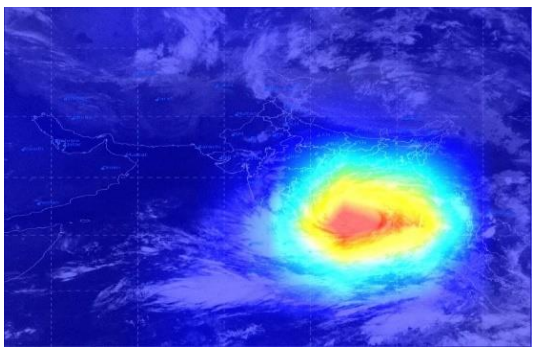

Figure 30. Localisation of Eye - Tropical Cyclone (TC) YAAS image using proposed Model and Grad – CAM technique

Grad-CAM (Gradient class activation mapping) creates a coarse localization map by utilising the gradients of any image of Tropical cyclonic cloud distribution flowing into the final convolutional layer in order to predict the eye of the storm. The Class Activation Map (CAM) is produced by Grad-CAM method using the activations from the final convolutional layer. By applying methods such as Guided Back-propagation, the visualization is improved to produce high-resolution detailed visualisations and localization that is discriminative based on class, which facilitate the interpretation of neural net decisions. Figure 30 shows localization of cyclonic storm eye.

5. CONCLUSION AND FUTURE SCOPE

A comprehensive assessment of the classification and detection approach for satellite tropical cyclone cloud distribution detection is provided in the results section and graphing of performance metrics against image dataset, including multiple Deep Neural Networks (DNN) is shown with respect to plots. Further using EfficientNetV2 Deep Neural Network an accuracy of 98% was attained on average by the algorithm during testing phase. Future iterations of the work will also include the identification of tropical cyclones using advanced deep learning techniques in conjunction with GPU capabilities of cloud computing.

Further research could concentrate on incorporating physics-based principles directly into the learning process of Deep neural networks, resulting in more accurate and physically realistic predictions, particularly in convective cloud development, climate modeling, Furthermore, combining data-driven approaches with physics-informed neural networks (PINNs) could result in hybrid models that outperform traditional CNNs in areas where they may struggle, improving generalization in complex scenarios. Furthermore, incorporating physics-based transformations into data augmentation techniques can provide a new level of robustness

and generalization, allowing networks such as Efficient-Net to generalize more effectively across a variety of real-world scenarios.

Using neural networks Cyclone forecasters can analyze massive amounts of historical weather data, satellite images, and other meteorological inputs to identify patterns that indicate the formation and progression of cyclones. Numerous factors influence cyclone development, including sea surface temperatures, atmospheric pressure, and wind patterns. Neural networks outperform traditional statistical methods in modelling the non-linear relationships between these variables, resulting in more accurate predictions of cyclone paths, intensity, and landfall. Cyclone forecasting and warning systems benefit significantly from neural networks because they improve prediction accuracy, allow for real-time data processing, and support effective early warning systems. They help to reduce the impact of cyclones on people and property, resulting in more resilient communities.

ACKNOWLEDGEMENTS

We are grateful to Dr. Mrutyunjay Mohapatra, Director General of Meteorology (DGM), India Meteorological Department (IMD), and Dr. S. Balachandran, DDGM, RMC-Chennai, IMD, for their continuous support and encouragement during the course of our work. Additionally, we would like to sincerely thank the RSMC & SATMET-Division in New Delhi for their support in the preparation of this paper. We are also grateful to the Indian space exploration agency ISRO, DWR-Chennai, DWR-Machilipatnam, and INSAT-3D and 3DR imagery, as well as the Doppler Weather Radar (DWR) at Cox's Bazar, Bangladesh, and Kyaukpyu, Myanmar for providing images during the evaluation of this model.

REFERENCES

[1] Mohapatra, M., Bandyopadhyay, B.K., Rathore, L.S. (2017). Tropical Cyclone Activity over the North Indian Ocean. Springer. https://doi.org/10.1007/978-3-319-40576-6

[2] Mohanty, U.C., Gopalakrishnan, S. (2016). Advanced Numerical Modeling and Data Assimilation Techniques for Tropical Cyclone Prediction. Springer. https://doi.org/10.5822/978-94-024-0896-6

[3] Ray, K., Mohapatra, M., Bandyopadhyay, B., Rathore, L. (2014). High-Impact Weather Events over the SAARC Region. Springer. https://doi.org/10.1007/978-3-319-10217-7

[4] Mohapatra, M., Bandyopadhyay, B., Nayak, D. (2013). Evaluation of operational tropical cyclone intensity forecasts over north Indian Ocean issued by India Meteorological Department. Natural Hazards, 68(2): 433-451. https://doi.org/10.1007/s11069-013-0624-z

[5] Alhichri, H., Alsuwayed, A., Bazi, Y., Ammour, N., Alajlan, N. (2021). Classification of remote sensing images using EfficientNet-B3 CNN model with attention. IEEE Access, 9: 14653-14668. https://doi.org/10.1109/ACCESS.2021.3051085

[6] Yamashita, R., Nishio, M., Do, R.K.G., Togashi, K. (2018). Convolutional neural networks: An overview and application in radiology. Insights into Imaging, 9: 611-629. https://doi.org/10.1007/s13244-018-0639-9

[7] Kotal, S.D., Bhattacharya, S.K. (2022). Improvement of displacement error of rainfall and wind field forecast associated with land falling tropical cyclone AMPHAN. Tropical Cyclone Research and Review, 11(3): 146-162. https://doi.org/10.1016/j.tcrr.2022.09.004

[8] Gupta, R.K., Jain, A., Wang, J., Singh, V.P., Bharti, S. (2022). Artificial intelligence of things for weather forecasting and climatic behavioral analysis. In Advances in Computational Intelligence and Robotics Book Series. https://doi.org/10.4018/978-1-6684-3981-4

[9] Aykat, S., Senan, S. (2023). Advanced detection of retinal diseases via novel hybrid deep learning approach. Traitement du Signal, 40(6): 2367-2382. https://doi.org/10.18280/ts.400604

[10] Gardoll, S., Boucher, O. (2022). Classification of tropical cyclone containing images using a convolutional neural network: Performance and sensitivity to the learning dataset. Geoscientific Model Development, 15: 7051-7073. https://doi.org/10.5194/gmd-15-7051-2022

[11] Wang, H., Xu, Q., Yin, X., Cheng, Y. (2024). Determination of low-intensity tropical cyclone centers in geostationary satellite images using a physics-enhanced deep-learning model. IEEE Transactions on Geoscience and Remote Sensing, 62: 4202810. https://doi.org/10.1109/TGRS.2024.3363842

[12] Aghazadeh, F., Ghasemi, M., Garajeh, M.K., Feizizadeh, B., Karimzadeh, S., Morsali, R. (2023). An integrated approach of deep learning convolutional neural network and google earth engine for salt storm monitoring and mapping. Atmospheric Pollution Research, 14(3): 101689. https://doi.org/10.1016/j.apr.2023.101689

[13] Ahmed, R., Prakash, S., Mohapatra, M., Giri, R.K., Dwivedi, S. (2022). Understanding the rapid intensification of extremely severe cyclonic storm 'Tauktae' using remote-sensing observations. Meteorology and Atmospheric Physics, 134(6). https://doi.org/10.1007/s00703-022-00935-0

[14] Patil, C., Malap, N., Sathyanadh, A., Balaji, B., Prabhakaran, T., Karipot, A. (2022). Moisture transport enhanced by the nocturnal low-level jet in association with the passage of a monsoon depression over the Indian subcontinent. Atmospheric Research, 272: 106123. https://doi.org/10.1016/j.atmosres.2022.106123

[15] Gurram, P., Kwon, H. (2013). Sparse kernel-based ensemble learning with fully optimized kernel parameters for hyperspectral classification problems. IEEE Transactions on Geoscience and Remote Sensing, 51(2): 787-802. https://doi.org/10.1109/TGRS.2012.2203603

[16] Sharma, A., Liu, X., Yang, X., Shi, D. (2017). A patch-based convolutional neural network for remote sensing image classification. Neural Networks, 95: 19-28. https://doi.org/10.1016/j.neunet.2017.07.017

[17] Pang, S., Xie, P., Xu, D., Meng, F., Tao, X., Li, B., Li, Y., Song, T. (2021). NDFTC: A new detection framework of tropical cyclones from meteorological satellite images with deep transfer learning. Remote Sensing,13(9): 1860. https://doi.org/10.3390/rs13091860

[18] Zheng, Z., Zhou, J., Gan, J., Luo, S., Gao, W. (2022). Fine-grained image classification based on cross-attention network. International Journal of Semantic Web and Information Systems, 18(1): 1-12. http://doi.org/10.4018/IJSWIS.315747

[19] Tan, M., Le, Q. (2019). EfficientNet: Rethinking model scaling for convolutional neural networks. In

Proceedings of the International Conference on Machine Learning, pp. 6105-6114. http://proceedings.mlr.press/v97/tan19a.html.
[20] Shakya, S., Kumar, S., Goswami, M. (2020). Deep learning algorithm for satellite imaging based cyclone detection. IEEE Journal of Selected Topics in Applied Earth Observations and Remote Sensing, 13: 827-839. https://doi.org/10.1109/JSTARS.2020.2970253
[21] Zhang, H., Song, H., Yu, B. (2011). Application of hyper spectral remote sensing for urban forestry monitoring in natural disaster zones. In 2011 International Conference on Computer and Management (CAMAN), Wuhan, China, pp. 1-4. https://doi.org/10.1109/CAMAN.2011.5778867
[22] Li, J., Huang, X., Gong, J. (2019). Deep neural network for remote-sensing image interpretation: Status and perspectives. National Science Review, 6(6): 1082-1086. https://doi.org/10.1093/nsr/nwz058
[23] Pradhan, R., Aygun, R. S., Maskey, M., Ramachandran, R., Cecil, D.J. (2018). Tropical cyclone intensity estimation using a deep convolutional neural network. IEEE Transactions on Image Processing, 27(2): 692-702. https://doi.org/10.1109/TIP.2017.2766358
[24] Jiang, H., Peng, M., Zhong, Y., Xie, H., Hao, Z., Lin, J., Ma, X., Hu, X. (2022). A survey on deep learning-based change detection from high-resolution remote sensing images. Remote Sensing, 14(7): 1552. https://doi.org/10.3390/rs14071552
[25] Sakaino, H., Gaviphatt, N., Insisiengmay, A., Zamora, L., Ningrum, D.F., Kotsuki, S. (2023). DeepTrCy: Life stage identification of satellite tropical cyclone images. In IGARSS 2023 - 2023 IEEE International Geoscience and Remote Sensing Symposium, Pasadena, CA, USA, pp. 5186-5189. https://doi.org/10.1109/IGARSS52108.2023.10282363
[26] Zheng, Z., Hu, C., Liu, Z., Hao, J., Hou, Q., Jiang, X. (2022). Deep learning for typhoon intensity classification using satellite cloud images. Journal of Atmospheric and Oceanic Technology, 39(1): 55-69. https://doi.org/10.1175/JTECH-D-19-0207.1
[27] Tan, M., Le, Q. (2021). EfficientNetV2: Smaller models and faster training. https://arxiv.org/abs/2104.00298
[28] Joseph, P.V. (1994). Tropical cyclone hazards and warning and disaster mitigation systems in India. Sādhanā, 19(4): 551-566. https://doi.org/10.1007/bf02835639
[29] Kumler-Bonfanti, C., Stewart, J., Hall, D., Govett, M. (2020). Tropical and extratropical cyclone detection using deep learning. Journal of Applied Meteorology and Climatology, 59: 1971-1985. https://doi.org/10.1175/JAMC-D-20-0117.1
[30] Chen, B., Chen, B., Lin, H., Elsberry, R.L. (2019). Estimating tropical cyclone intensity by satellite imagery utilizing convolutional neural networks. Weather and Forecasting, 34: 447-465. https://doi.org/10.1175/WAF-D-18-0136.1
[31] Bourdin, S., Fromang, S., Dulac, W., Cattiaux, J., Chauvin, F. (2022). Intercomparison of four algorithms for detecting tropical cyclones using ERA5. Geoscientific Model Development, 15(17): 6759-6786. https://doi.org/10.5194/gmd-15-6759-2022
[32] Rajesh, K., Ramaswamy, V., Kannan, K., Arunkumar, N. (2019). Satellite cloud image classification for cyclone prediction using dichotomous logistic regression based fuzzy hypergraph model. Future Generation Computer Systems, 98: 688-696. https://doi.org/10.1016/j.future.2018.12.042
[33] Dvorak, V.F. (1975). Tropical cyclone intensity analysis and forecasting from satellite imagery. Monthly Weather Review, 103: 420-430. https://doi.org/10.1175/15200493(1975)103,0420:TCIAAF.2.0.CO;2
[34] Maskey, M., Ramachandran, R., Ramasubramanian, M., Gurung, I., Freitag, B., Kaulfus, A. (2020). Deepti: Deep-learning-based tropical cyclone intensity estimation system. IEEE Journal of Selected Topics in Applied Earth Observations and Remote Sensing, 13: 4271-4281. https://doi.org/10.1109/jstars.2020.3011907
[35] Jergensen, G.E., McGovern, A., Lagerquist, R., Smith, T. (2020). Classifying convective storms using machine learning. Weather and Forecasting, 35: 537-559. https://doi.org/10.1175/WAF-D-19-0170.1
[36] Tao, Y., Xu, M., Zhang, F., Du, B., Zhang, L. (2017). Unsupervised-restricted deconvolutional neural network for very high resolution remote-sensing image classification. IEEE Transactions on Geoscience and Remote Sensing, 55(12): 6805-6823. https://doi.org/10.1109/TGRS.2017.2734697
[37] Merrill, R.T. (1993). Tropical cyclone structure. Global Guide to Tropical Cyclone Forecasting. https://cyclone.wmo.int/pdf/Global-Guide-to-Tropical-Cyclone-Forecasting.pdf.
[38] Jaiswal, N., Kishtawal, C. M. (2013). Objective detection of center of tropical cyclone in remotely sensed infrared images. IEEE Journal of Selected Topics in Applied Earth Observations Remote Sensing, 6(2): 1031-1035. https://doi.org/10.1109/JSTARS.2012.2215016
[39] Wimmers, A., Velden, C., Cossuth, J.H. (2019). Using deep learning to estimate tropical cyclone intensity from satellite passive microwave imagery. Monthly Weather Review, 147(6): 2261-2282. https://doi.org/10.1175/mwr-d-18-0391.1
[40] Schmit, T., Lindstrom, S., Gerth, J.J., Gunshor, M. (2018). Applications of the 16 spectral bands on the Advanced Baseline Imager (ABI). Journal Operational Meteorology, 6: 33-46, https://doi.org/10.15191/nwajom.2018.0604
[41] Lagerquist, R., Stewatt, J.Q., Ebert-Uphoff, I., Kumler, C. (2021). Using deep learning to nowcast the spatial coverage of convection from Himawari-8 satellite data. Monthly Weather Review, 149(12): 3897-3921. https://doi.org/10.1175/mwr-d-21-0096.1
[42] Malakar, P., Kesarkar, A.P., Bhate, J.N., Singh, V., Deshamukhya, A. (2020). Comparison of reanalysis data sets to comprehend the evolution of tropical cyclones over North Indian Ocean. Earth and Space Science, 7(2). https://doi.org/10.1029/2019ea000978
[43] Prabhat, Kashinath, K., Mudigonda, M., Kim, S., Kapp-Schwoerer, L., et al. (2021). ClimateNet: An expert-labeled open dataset and deep learning architecture for enabling high-precision analyses of extreme weather. Geoscientific Model Development, 14: 107-124. https://doi.org/10.5194/gmd-14-107-2021
[44] Selvaraju, R.R., Cogswell, M., Das, A. (2020). Grad-CAM: Visual explanations from deep networks via gradient-based localization. International Journal of Computer-Vision, 128: 336-359. https://doi.org/10.1007/s11263-019-01228-7